Available online at www.sciencedirect.com
SCIENCE DIRECT
Journal of Photochemistry and Photobiology A: Chemistry 176 (2005) 114–123
Journal of Photochemistry and Photobiology A:Chemistry
www.elsevier.com/locate/jphotochem

Spectroscopic and kinetic study of the gas-phase CS_2–Cl adduct

V. Dookwah-Roberts [a], R. Soller [b], J.M. Nicovich [b], P.H. Wine [a,b,*]

[a] *School of Earth and Atmospheric Sciences, Georgia Institute of Technology, Atlanta, GA 30332, USA*
[b] *School of Chemistry and Biochemistry, Georgia Institute of Technology, Atlanta, GA 30332, USA*

Available online 12 September 2005

Abstract

Time-resolved UV–vis absorption spectroscopy (TRUVVAS) has been coupled with 248 nm laser flash photolysis (LFP) of Cl_2CO in the presence of CS_2 (and in some cases O_2, NO or NO_2) to generate the CS_2–Cl radical adduct in the gas phase and study the spectroscopy and kinetics of this species. CS_2–Cl is found to possess a strong absorption band at $\lambda_{max} \approx 365$ nm with $\sigma_{max} = (2.3 \pm 0.7) \times 10^{-17}$ cm^2 molecule^{-1} (base e) and a weaker band at $\lambda_{max} \approx 480$ nm; the gas-phase spectrum of CS_2–Cl is very similar to the previously reported liquid-phase spectrum in CCl_4 solvent. Reaction of CS_2–Cl with O_2 is found to be very slow; our data suggest that the rate coefficient for this reaction at 240 K is less than 5.0×10^{-18} cm^3 molecule^{-1} s^{-1}. Rate coefficients for CS_2–Cl reactions with CS_2–Cl (k_3), NO (k_5), and NO_2 (k_6) were measured at 240 K and, in units of 10^{-11} cm^3 molecule^{-1} s^{-1}, were found to be $2k_3 = 15 \pm 6$, $k_5 = 2.2 \pm 0.5$, and $k_6 = 1.3 \pm 0.4$, where the uncertainties are estimates of accuracy at the 95% confidence level.

Keywords: Atmosphere; Sulfur; Photo-chlorination

1. Introduction

The existence of an addition complex between CS_2 and atomic chlorine was first postulated in the 1950s to explain how use of CS_2 as solvent in studies of liquid-phase photochlorination reactions dramatically increases the selectivity for tertiary versus primary hydrogen abstraction [1–3]. Several decades after its existence was first postulated, a CS_2–Cl adduct in CCl_4 solvent was observed by Chateauneuf [4] using UV–vis spectroscopy as the detection technique. The observed liquid phase spectrum has a strong absorption feature at $\lambda \sim 370$ nm and a weaker feature at $\lambda \sim 490$ nm [4]. Based on the data obtained using both the pulse radiolysis and laser flash photolysis (LFP) techniques, Chateauneuf reported a rate coefficient of 1.7×10^{10} M^{-1} s^{-1} for the liquid-phase addition of Cl to CS_2 and an equilibrium constant of 1900 M^{-1} for $Cl + CS_2 \leftrightarrow CS_2$–Cl [4]. The resonance Raman spectrum of CS_2–Cl in CCl_4 solvent has been observed by Wang et al. [5] using an excitation wavelength (369 nm) that is in resonance with the strong absorption band. Comparison of observed vibrational frequencies with those obtained from electronic structure calculations suggests that the complex formed by the addition of Cl to CS_2 is SCS–Cl, not S_2C–Cl as had been suggested by earlier theoretical studies [6–8]. Similar conclusions have been reached concerning the structure of CS_2–OH, which has been studied extensively in the gas phase because of its importance in atmospheric chemistry [9–24]. A recent theoretical study of CS_2–Cl complexes and their isomerization reactions [25] reports that (i) formation of SCS–Cl is essentially a barrierless process, whereas formation of S_2C–Cl has a barrier of 74 kJ mol^{-1}; (ii) the 0 K bond dissociation energies for SCS–Cl and S_2C–Cl are 33 kJ mol^{-1} and 28 kJ mol^{-1}, respectively; (iii) the barrier for isomerization of SCS–Cl to S_2C–Cl is 55 kJ mol^{-1}; and (iv) the isomerization barrier is reduced to 11 kJ mol^{-1} in the presence of Cl atoms via formation of a low-energy transition state with Cl atoms weakly attached to both the carbon atom and one of the sulfur atoms.

Interest in the atmospheric chemistry of CS_2 centers around its role as a source of OCS, the longest-lived and most concentrated atmospheric sulfur species [26,27]; transport of OCS to the lower stratosphere followed by photolysis

* Corresponding author. Tel.: +1 404 894 0400; fax: +1 404 894 7452.
E-mail address: paul.wine@chemistry.gatech.edu (P.H. Wine).

1010-6030/$ – see front matter © 2005 Elsevier B.V. All rights reserved.
doi:10.1016/j.jphotochem.2005.08.013

and oxidation of the photolytically-generated sulfur atoms is thought to be an important source of the persistent sulfate aerosol layer in the lower stratosphere [26,28,29]. While CS_2 oxidation in the atmosphere is thought to be dominated by reaction with the OH radical [26,27,30], the gas-phase reaction of atomic chlorine with CS_2 has been studied experimentally because of its potential importance as an additional atmospheric sink for CS_2. Martin et al. [31], employing a competitive kinetics technique, found that in the presence of O_2 the apparent bimolecular rate coefficient for destruction of CS_2 by Cl is of the order 10^{-13} cm^3 molecule^{-1} s^{-1} and, in 1 atm $N_2 + O_2$ at 293 K, increases by nearly a factor of three as the O_2 partial pressure increases from 50 to 760 Torr. Martin et al. interpreted their results in terms of a mechanism that is analogous to the generally accepted mechanism for OH + CS_2 reaction, i.e., formation of a weakly-bound CS_2–Cl adduct that reacts with O_2 in competition with decomposition back to reactants:

$$Cl + CS_2 + M \rightarrow CS_2{-}Cl + M \quad (1)$$

$$CS_2{-}Cl + M \rightarrow Cl + CS_2 + M \quad (-1)$$

$$CS_2{-}Cl + O_2 \rightarrow \text{products} \quad (2)$$

Nicovich et al. [32] employed the laser flash photolysis–resonance fluorescence (LFP–RF) technique to directly confirm the occurrence of reactions (1) and (-1). Rate coefficients for reactions (1) and (-1) were determined as a function of temperature and pressure over the ranges 193–258 K and 30–600 Torr N_2. From the temperature dependence of k_1/k_{-1}, Nicovich et al. were able to deduce a 0 K adduct bond dissociation energy of 40 ± 3 kJ mol^{-1}, in reasonable agreement with the recently reported theoretical SCS–Cl bond dissociation energy of 33 kJ mol^{-1} [25]. Based on the observation of the dependence of observed Cl temporal profiles on [O_2], Nicovich et al. concluded that $k_2 < 2 \times 10^{-15}$ cm^3 molecule^{-1} s^{-1} at $T = 230$ K and $P = 30$ Torr O_2. Wallington et al. [33] studied the gas-phase Cl + CS_2 reaction using an experimental approach similar to the one employed by Martin et al. [31]. These investigators concluded that the overall reaction was much slower than that reported by Martin et al. ($k < 4 \times 10^{-15}$ cm^3 molecule^{-1} s^{-1}) and suggested that the loss of CS_2 observed in the Martin et al. study was not the result of Cl + CS_2 + O_2 reaction, but rather the result of OH + CS_2 + O_2 reaction, with OH generated primarily by the secondary reaction of Cl with CH_3OOH.

In this paper we report the results of an experimental study of the gas-phase Cl + CS_2 reaction that couples LFP with time-resolved UV–vis absorption spectroscopy (TRUVVAS). The gas-phase absorption spectrum of the CS_2–Cl adduct is reported for the first time, and the TRUVVAS technique is used as a probe to investigate the kinetics of CS_2–Cl reactions with O_2, NO, NO_2, and CS_2–Cl. As expected, based on the results of Wallington et al. [33], CS_2–Cl is found to be of little importance in atmospheric chemistry. However, the results reported in this study are useful for developing an understanding of (i) the kinetics and spectroscopy of gas-phase adducts of radicals with sulfur compounds; and (ii) differences (or similarities) between gas- and liquid-phase adduct spectroscopy and kinetics.

2. Experimental technique

The LFP–TRUVVAS apparatus used in this study is similar to the one we employed in a spectroscopic and kinetic study of the Cl–S$(CH_3)_2$ adduct [34]. A schematic diagram of the apparatus is shown in Fig. 1. Major elements of the apparatus include a pulsed KrF photolysis laser (248 nm), a 75 Watt xenon arc lamp cw probe light source, an insulated Pyrex, jacketed reaction cell (100 cm long, 40 mm i.d.), a pre-mixing and pre-cooling cell, a monochromator to isolate the probe wavelength, a photomultiplier tube (PMT) to detect the probe radiation, an oscilloscope to record the temporal evolution of the transmitted probe radiation, a computer to store and average the waveforms from the oscilloscope, and numerous optical components to manipulate and align the photolysis and probe beams. As depicted in Fig. 1, the UV–vis probe beam was directed through the reaction cell to overlap collinearly with the photolysis beam. The monochromator entrance and exit slits were set at 1.5 mm, providing a spectral resolution of 5.5 nm (full width at half maximum; FWHM).

The reaction and pre-mixing cell were surrounded by an insulated Pyrex jacket through which ethanol was flowed from a reservoir, enabling the cell temperature to be controlled. The temperatures of the reaction gas mixture near the two ends of the cell were measured with thermocouples. The temperature gradient between the ends of the cell was typically ± 2 K, and the average of the temperatures measured at the two ends was taken to be the cell temperature. Dry nitrogen gas was sprayed on the quartz cell windows to prevent condensation of water vapor when the cell was cooled.

The CS_2–Cl adduct was generated by photolyzing Cl_2CO in the presence of CS_2. The absorption cross-section for Cl_2CO at 248 nm is 8.93×10^{-20} cm^2 molecule^{-1} [35], and the typical photolysis fluence was ~20 mJ cm^{-2} pulse^{-1}; the pulse duration was ~25 ns.

All experiments were carried out under "slow-flow" conditions, i.e., the linear flow rate of the reaction mixture through the reaction cell (typically 10 cm s^{-1}) was fast enough to replenish the volume of the reaction cell between photolysis laser pulses (typical laser repetition rate was 0.14 Hz), but slow enough that kinetic observations could be analyzed assuming static conditions. Concentrations of both CS_2 and Cl_2CO were measured in situ in the slow-flow system by UV photometry at 213.9 nm (Zn penray lamp light sources) and by mass flow measurements. In units of 10^{-19} cm^2 molecule^{-1}, the cross-sections used to convert 213.9 nm absorbances to concentrations were 36 [36]

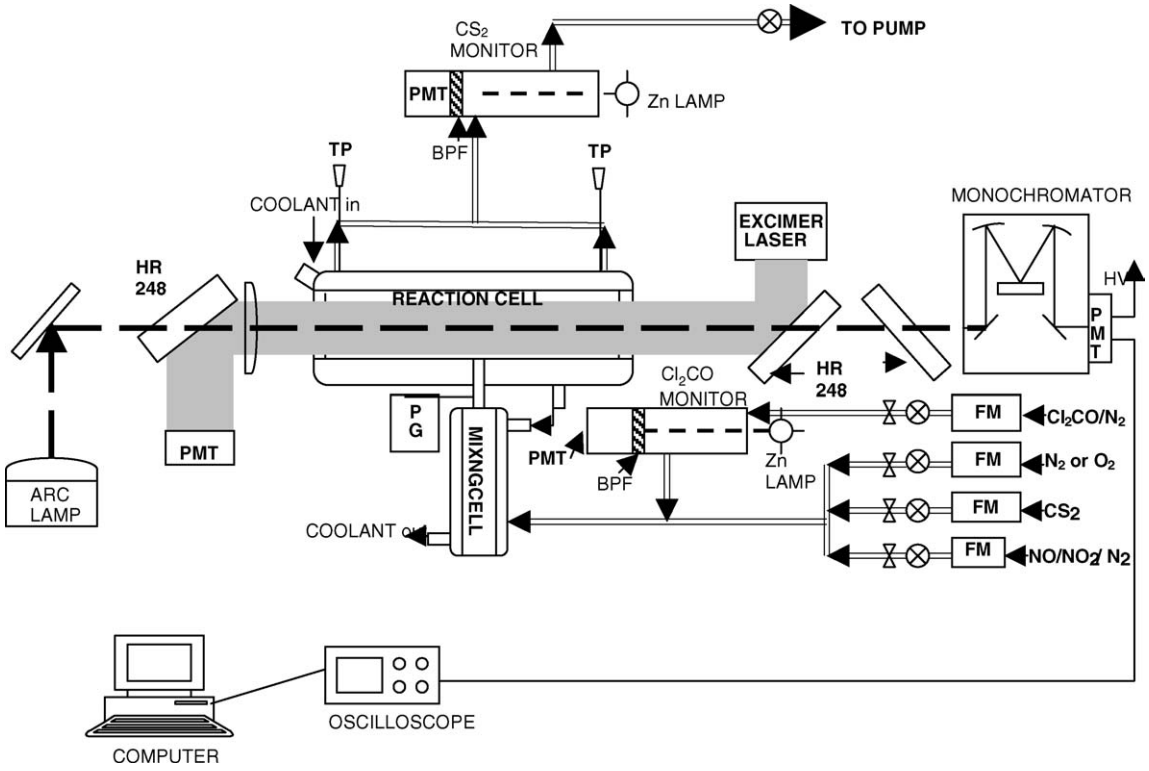

Fig. 1. Laser flash photolysis/UV–vis absorption spectroscopy apparatus: HR 248, high reflectivity 248 nm mirror; PMT, photomultiplier tube; BPF, band pass filter; PM, power meter; PG, pressure gauge; FM, flow meter; TP, temperature probe.

and 1.26 [34] for CS_2 and Cl_2CO, respectively. The Cl_2CO absorption cell was 25 cm in length and was positioned upstream from the mixing chamber; the mixing dilution factor was determined from mass flow measurements. The CS_2 absorption cell was 5.6 cm in length and was positioned downstream from the mixing chamber; correction for Cl_2CO absorbance was made based on the dilution-corrected upstream absorption measurements in the 25 cm cell. In the kinetics experiments, the concentrations of NO and NO_2 were determined from mass flow measurements. A certified NO/N_2 mixture (Matheson, 1.87% NO) was used to supply NO. Nitrogen dioxide was transferred into a 12 L Pyrex bulb and diluted with O_2. The NO_2 mole fraction of the NO_2/O_2 mixture was measured frequently using UV photometry at 366 nm (Hg penray lamp light source); the absorption cross-section used to convert measured absorbances to NO_2 concentrations was 6.05×10^{-19} cm^2 $molecule^{-1}$ [37]. The pure gases used in this study were obtained from Air Products (O_2, N_2) and Matheson (Cl_2CO, NO_2), and had the following stated minimum purities: N_2, 99.999%; O_2, 99.994%; Cl_2CO, 99.0%; and NO_2, 99.5%. The N_2, O_2, and NO_2, were used as supplied. The Cl_2CO was degassed at 77 K prior to use. HPLC grade carbon disulfide (Aldrich) had a stated minimum purity of 99.9+%. The carbon disulfide was transferred under N_2 into a vial fitted with a high-vacuum stopcock and degassed repeatedly at 77 K before use.

3. Results and discussion

When Cl_2CO was photolyzed in the presence of CS_2, absorption of the UV–vis probe beam was observed throughout the 320–550 nm spectral region. Absorption was observed only when both CS_2 and Cl_2CO were simultaneously subjected to LFP. When the photolyzed mixture contained only Cl_2CO, CS_2, and N_2, the observed absorbance (A) decayed slowly with time according to second-order kinetics. Under the experimental conditions employed, the appearance of absorbance was very fast compared to the decay of absorbance. Hence, the peak absorbance for each experiment could be determined with good accuracy by plotting A^{-1} versus time and extrapolating back to $t = 0$ using a linear fit to the A^{-1} versus time data.

3.1. Adduct identification

Evidence verifying the identity of the absorbing species was obtained by measuring its appearance rate. Absorbance temporal profiles were recorded and analyzed using a non-linear least squares fit to the sum of an exponential rise and decay (see Fig. 2). In this set of experiments, absorbance disappearance resulted primarily from radical–radical reactions and was not a first-order process. The first-order absorbance disappearance rate, k_d, is thus a parameterized rate coefficient rather than the sum of actual loss processes that are

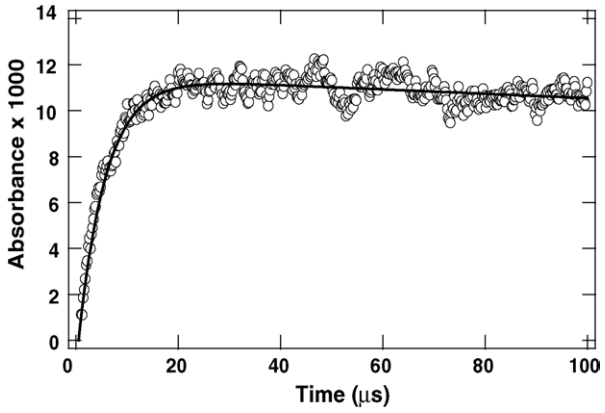

Fig. 2. Typical absorbance (base e) temporal profile observed following laser flash photolysis of $Cl_2CO/CS_2/N_2$ mixtures. Experimental conditions: $T = 240$ K; $P = 100$ Torr; concentrations in units of 10^{13} molecules cm^{-3} are $[CS_2] = 1870$, $[Cl_2CO] = 900$, and $[Cl]_0 \approx 0.5$. The solid line is obtained from a nonlinear least squares fit of the data to the sum of an exponential rise and decay. Best fit appearance (k_a) and disappearance (k_d) rate coefficients in units of s^{-1} are $k_a = 1.30 \times 10^5$ and $k_d = 804$.

quantitatively attributable to specific first-order processes. However, because the observed absorbance loss rates are slow compared to the rapid rate of absorbance appearance, the parameterization of the absorbance disappearance as a first-order process does not seriously impact the reliability of the analysis to determine the pseudo-first-order rate coefficient for absorbance appearance. As shown by the example in Fig. 2, the quality of the double exponential fits is quite good as long as the fit is limited to a small fraction of the decay. Pseudo-first-order appearance rate coefficients (k_a) were measured at 365 nm in N_2 buffer gas. As shown in Fig. 3, a plot of k_a versus $[CS_2]$ is linear over the range of CS_2 concentrations employed. The linearity of the k_a versus $[CS_2]$ plot up to the fastest appearance rate measured (ca. 300,000 s^{-1}) demonstrates that the rate-limiting step in the production of the absorbing species is

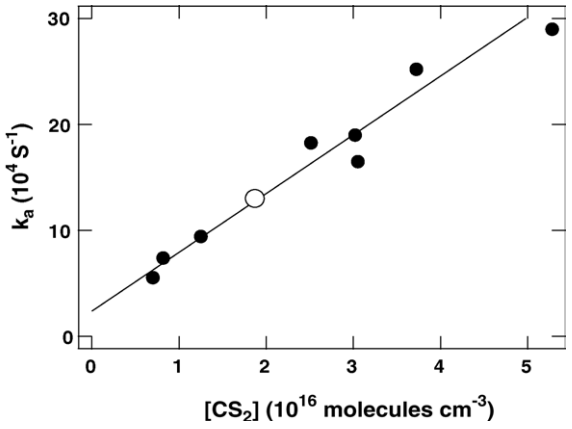

Fig. 3. Plot of k_a vs. $[CS_2]$ for data obtained at $T = 240$ K and $P = 100$ Torr N_2. The solid line is obtained from a linear least squares analysis; its slope gives the second-order rate coefficient $(5.20 \pm 0.84) \times 10^{-12}$ cm^3 $molecule^{-1}$ s^{-1} where the uncertainty is 2σ and represents precision only. The open data point is the one obtained from the data shown in Fig. 2.

the $Cl + CS_2$ reaction under the conditions investigated. The slope of the k_a versus $[CS_2]$ plot yields the second-order rate coefficient $k_1 = (5.2 \pm 0.8) \times 10^{-12}$ cm^3 $molecule^{-1}$ s^{-1} at 240 K and 100 Torr total pressure, where the uncertainty is 2σ and represents precision only. The value measured here for $k_1(P, T)$ is in good agreement with the value $(4.8 \pm 0.3) \times 10^{-12}$ cm^3 $molecule^{-1}$ s^{-1} reported by Nicovich et al. [32] based on measurements of Cl atom decay using atomic resonance fluorescence spectroscopy as the detection technique. As expected since $k_a = k_1[CS_2] + k_{-1}$, the intercept of the k_a versus $[CS_2]$ plot is very close to the value k_{-1} (240 K, 100 Torr N_2) $\sim 32{,}000$ s^{-1} reported by Nicovich et al. [32]. The data in Figs. 2 and 3 provide strong evidence that the species being observed is indeed the CS_2–Cl adduct formed from the reaction of Cl with CS_2.

The liquid phase $Cl + CS_2$ rate coefficient of 1.7×10^{10} M^{-1} s^{-1} reported by Chateauneuf [4] is very near the diffusion-controlled limit, while the rate coefficient obtained in this study is about a factor of 50 below the gas kinetic limit. Although solvent effects undoubtedly play some role in the liquid phase kinetics, the most important factor accounting for the difference in observed rate coefficients is probably that liquid-phase conditions are equivalent to the gas-phase high pressure limit, which is not approached at pressures where gas-phase kinetic data for reaction (1) are available. In fact, the pressure dependence results reported by Nicovich et al. [32] suggest that $k_1(P, T)$ is much closer to the low pressure limit than it is to the high pressure limit at $T = 240$ K and $P = 100$ Torr N_2.

3.2. Adduct absorption spectrum

The absorption spectrum of CS_2–Cl adduct was measured at 100 Torr total pressure (N_2 buffer) and 240 K. A reference wavelength of 365 nm was selected. Absorption measurements were made at this reference wavelength after every five measurements at other wavelengths. This was done in order to account for systematic drifts in experimental parameters, such as laser power, $[Cl_2CO]$, optical alignment, etc. over time. Absorbance measurements at wavelengths other than 365 nm were normalized to the average of the "before" and "after" 365 nm absorbances. The adduct absorption cross-section was carefully measured at 365 nm, and all cross-sections were then determined by applying the normalization factor to the carefully measured reference cross-section.

Reagent concentrations employed in the 365 nm cross-section measurements at 240 K were (in units of 10^{13} molecules cm^{-3}): $[CS_2] \approx 7000$; $[Cl_2CO] = 5$–200; $[Cl]_0 = 0.05$–2. Values for A_0 (defined below) were obtained by extrapolation of A^{-1} versus time (t) data to $t = 0$. High CS_2 concentrations were employed in order to obtain ~95% conversion of Cl to CS_2–Cl at equilibrium (based on the equilibrium constants reported by Nicovich et al. [32]). Each cross-section measurement involved averaging ~50 photolysis laser pulses. To verify reproducibility, multiple absolute cross-section measurements at 365 nm and relative

cross-section measurements at other wavelengths were made over a period of several days. The adduct cross-section at 365 nm (σ_{365}) was determined from the data using the following relationship:

$$\sigma_{365} = \frac{A_0}{l[\mathrm{Cl}]_0 F} \quad \text{(I)}$$

In Eq. (I), A_0 is the absorbance at a time shortly after the laser flash when Cl and adduct have reached equilibrium but negligible radical decay has occurred, l the absorption path length (100 cm), $[\mathrm{Cl}]_0$ the concentration of chlorine atoms produced by the laser flash, and F the fraction of Cl atoms converted to adduct (taken to be the adduct equilibrium fraction). As typical for gas-phase spectroscopic data, the absorbance is defined as $A = \ln(I_0/I)$, i.e., it is a base e value. Cross-sections obtained from Eq. (I) were found to be independent of $[\mathrm{Cl}]_0$ over the range specified above, i.e., Beer's law was obeyed. Evaluation of $[\mathrm{Cl}]_0$ required (i) careful measurements of $[\mathrm{Cl_2CO}]$ and laser power; (ii) assumption of a quantum yield of 2.0 for production of Cl from 248 nm photolysis of $\mathrm{Cl_2CO}$; and (iii) careful measurements of the photolysis laser beam cross-sectional area and its divergence down the length of the cell (the laser beam area increased by a factor of 1.5 between the cell entrance and exit and was assumed to be the average of the entrance and exit areas for purposes of evaluating $[\mathrm{Cl}]_0$).

The assumption of a quantum yield of 2.0 for Cl atom production from $\mathrm{Cl_2CO}$ photolysis is based on strong experimental evidence that ClCO is not produced with significant yield as a stabilized photolysis product. Maul et al. [38] have studied the photo-dissociation dynamics of $\mathrm{Cl_2CO}$ using 235 nm pulsed laser excitation and resonance enhanced multiphoton ionisation (REMPI)–time of flight mass spectrometry (TOFMS) detection. Based on the analysis of kinetic energy release in the photolysis products, Maul et al. conclude that photo-dissociation of $\mathrm{Cl_2CO}$ occurs by concerted release of the three photofragments Cl + Cl + CO [38]. Temperature- and pressure-dependent rate coefficients for ClCO unimolecular dissociation are reported in literature [39]. Based on these rate coefficients, we expected to see evidence for slow Cl atom production after the photoflash in studies of low-temperature chlorine atom kinetics carried out in our laboratory, that employed 266 nm photolysis of $\mathrm{Cl_2CO}$ as the Cl source [40,41], if thermalized ClCO was produced as a photolysis product. Observed Cl atom temporal profiles following laser flash photolysis of $\mathrm{Cl_2CO/N_2}$ mixtures showed no evidence for Cl atom production by post-flash chemistry. As mentioned above, transient absorption was observed only when both $\mathrm{Cl_2CO}$ and $\mathrm{CS_2}$ were present in the reaction mixture. Hence, if ClCO was produced, it was not detected as an interfering absorber in this study.

The adduct spectrum measured in this study at $T = 240$ K and $P = 100$ Torr $\mathrm{N_2}$ is shown in Fig. 4, and is given in digitized form in Table 1. The $\mathrm{CS_2}$—Cl absorption spectrum was also measured at 298 K and was found to be identical to the spectrum obtained at 240 K within the precision

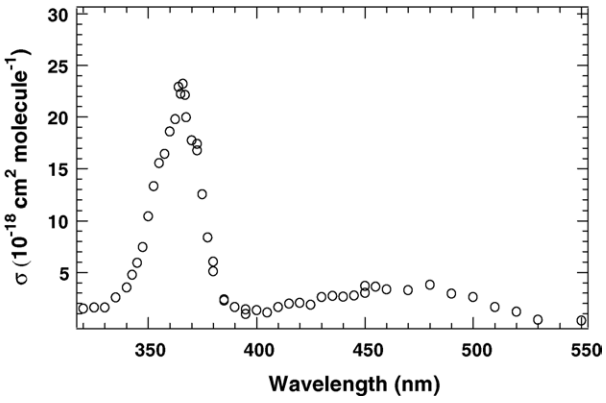

Fig. 4. Absorption spectrum of the $\mathrm{CS_2}$—Cl adduct.

Table 1
Absorption cross-sections for the $\mathrm{CS_2}$—Cl adduct as a function of wavelength at a spectral resolution of 5.5 nm FWHM[a]

λ	σ
320	1.56
325	1.67
330	1.66
335	2.68
340	3.68
345	6.17
350	10.86
355	16.17
360	19.36
365	23.20
370	18.48
375	13.05
380	6.29
385	2.35
390	1.72
395	1.47
400	1.41
405	1.18
410	1.70
415	2.07
420	2.12
425	1.95
430	2.73
435	2.83
440	2.77
445	2.86
450	3.13
455	3.76
460	3.49
470	3.42
480	3.94
490	3.07
500	2.73
510	1.71
520	1.26
530	0.44
550	0.33
600	0.19

[a] Units are λ (nm) and σ (10^{-18} $\mathrm{cm^2}$ $\mathrm{molecule^{-1}}$).

and accuracy of the measurements. The similarity between the gas-phase absorption spectrum reported in this study and the published liquid-phase spectrum [4] lends further support to our conclusion that the species observed in this study is the CS_2–Cl adduct. Consideration of uncertainties in the parameters that must be known to obtain the adduct cross-section (see above) leads to an estimate of ±30% for the accuracy of the measured cross-section at 365 nm (95% confidence level). We report this cross-section to be $\sigma_{365} \approx \sigma_{max} = (2.3 \pm 0.7) \times 10^{-17}$ cm^2 molecule^{-1}.

As discussed in Section 1, comparison of calculated vibrational frequencies for SCS–Cl and S_2C–Cl with frequencies measured using resonance Raman spectroscopy provides compelling evidence that the strong band at 365 nm results from absorption by SCS–Cl [5]. An important question that remains to be answered concerns the origin of the weak band observed at longer wavelength. Does this band result from promotion of ground state SCS–Cl to a lower-energy excited electronic state, or is it an absorption band of the S_2C–Cl isomer? Further experimental and theoretical research appears to be needed to answer this question. We have employed the theoretical energetics, structures, and vibrational frequencies reported by Phillips and co-workers [5,25] to evaluate the equilibrium constant for SCS–Cl ↔ S_2C–Cl. It appears that even if the initially generated SCS–Cl equilibrates rapidly with S_2C–Cl, only a few percent of the adduct molecules would exist as S_2C–Cl at the temperatures employed in our study. Hence, if the theoretical information is accurate, and if the weak long-wavelength band originates from S_2C–Cl, the peak absorption cross-section for this band, defined as σ (480 nm) ≈ $\sigma_{peak} = A_0(l[S_2C\text{–}Cl])^{-1}$ must be extremely large, i.e., approaching 10^{-16} cm^2 molecule^{-1}.

3.3. Radical–radical reaction kinetics

When reaction mixtures containing only Cl_2CO, CS_2, and N_2 are subjected to 248 nm laser flash photolysis and detectable levels of CS_2–Cl are generated, we expect that CS_2–Cl loss will be dominated by the following radical–radical reactions:

$$CS_2\text{–}Cl + CS_2\text{–}Cl \rightarrow \text{products} \quad (3)$$

$$Cl + CS_2\text{–}Cl \rightarrow \text{products} \quad (4)$$

In the limit of very high [CS_2], the ratio [CS_2–Cl]/[Cl] becomes large and reaction (3) is expected to dominate the adduct removal. As the CS_2 concentration is reduced, reaction (4) is expected to become an important adduct loss mechanism.

To experimentally determine k_3 at $T = 240$ K and $P = 100$ Torr, experiments were carried out using [CS_2] ~ 1×10^{17} molecules cm^{-3}; at this temperature and [CS_2], the ratio [CS_2–Cl]/[Cl] is approximately 24 [32]. The concentrations of Cl_2CO employed in these experiments were in the range (1.5–26) × 10^{15} molecules cm^{-3}, and values for $[Cl]_0$ were in the range (6–90) × 10^{12} atoms cm^{-3}. A typical

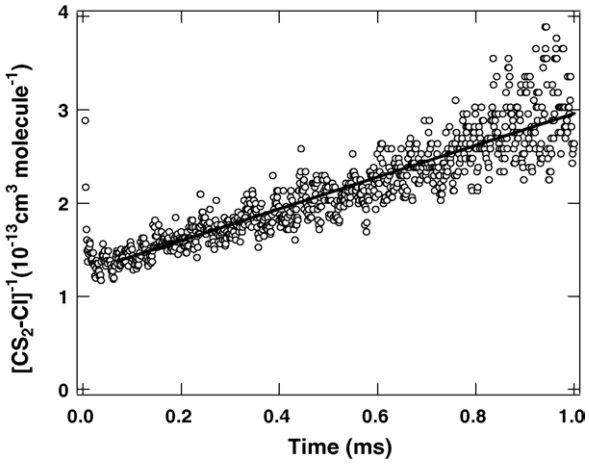

Fig. 5. CS_2–Cl absorbance temporal profile plotted as $[CS_2\text{–}Cl]^{-1}$ vs. time. Experimental conditions: $T = 240$ K; $P = 100$ Torr N_2; [CS_2] = 1.0×10^{17} molecules cm^{-3}. The solid line is obtained from a linear least squares analysis; its slope gives $2k_3 = (1.70 \pm 0.04) \times 10^{-10}$ cm^3 molecule^{-1} s^{-1} where the uncertainty is 2σ and represents precision only.

absorbance temporal profile, plotted as $[CS_2\text{–}Cl]^{-1}$ versus time, is shown in Fig. 5. The linearity of the $[CS_2\text{–}Cl]^{-1}$ versus time plot is consistent with the hypothesis that CS_2–Cl loss is dominated by reaction (3), and the self-reaction rate coefficient, $2k_3$, is obtained from the slope of the plot. The average of 17 experiments like the one depicted in Fig. 4 gives $2k_3 = (1.5 \pm 0.3) \times 10^{-10}$ cm^3 molecule^{-1} s^{-1}, where the uncertainty is 2σ and represents precision only. The accuracy of the derived value for $2k_3$ is limited by the accuracy of [CS_2–Cl], which in turn is limited by the accuracy of the CS_2–Cl absorption cross-section at the monitoring wavelength (365 nm), i.e., ±30% (see above). Taking the CS_2–Cl absorption cross-section and imprecision to be the two main sources of uncertainty, we report $2k_3 = (1.5 \pm 0.6) \times 10^{-10}$ cm^3 molecule^{-1} s^{-1}, where the uncertainty represents accuracy at the 95% confidence level.

In order to obtain information about k_4, it is necessary to employ experimental conditions where absorption signals are very low. Hence, it has not proven possible to obtain a quantitative value for k_4. Examination of the dependence of the CS_2–Cl disappearance rate on [CS_2] while keeping $[Cl]_0$ approximately constant does, however, suggest that $k_4 > k_3$.

3.4. Kinetics of the CS_2–Cl + O_2 reaction

To investigate the kinetics of the reaction of CS_2–Cl with O_2,

$$CS_2\text{–}Cl + O_2 \rightarrow \text{products} \quad (2)$$

CS_2–Cl absorbance temporal profiles were measured in 200 Torr of O_2 at $T = 240$ K with experimental conditions adjusted to relatively high [CS_2] and low $[Cl]_0$ in order to minimize the contribution of radical–radical reactions to CS_2–Cl removal. Temporal profiles observed in 200 Torr

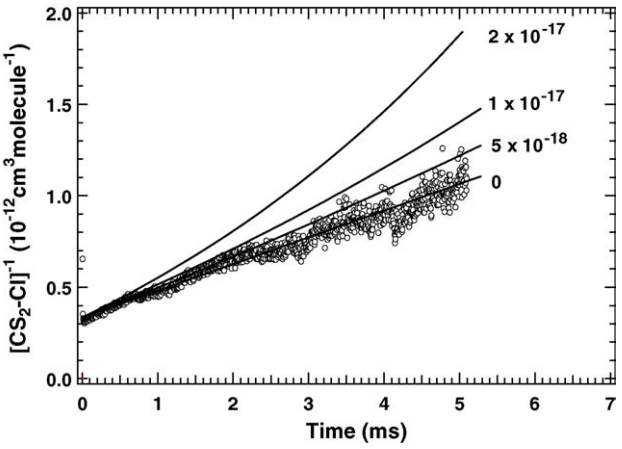

Fig. 6. CS_2–Cl absorbance temporal profile plotted as $[CS_2–Cl]^{-1}$ vs. time. Experimental conditions: $T = 240$ K; $P = 200$ Torr O_2; $[CS_2] = 6.1 \times 10^{16}$ molecules cm^{-3}; and $[Cl_2CO] = 7.4 \times 10^{14}$ molecules cm^{-3}. The straight line is obtained from a linear least squares analysis; its slope gives $2k_3 = (1.46 \pm 0.02) \times 10^{-10}$ cm^3 molecule^{-1} s^{-1} where the uncertainty is 2σ and represents precision only. The curved lines are simulations of the $[CS_2–Cl]^{-1}$ vs. time plots expected if k_2 had the values shown in the figure (in units of cm^3 molecule^{-1} s^{-1}).

O_2 were indistinguishable from those observed in N_2 bath gas; a plot of $[CS_2–Cl]^{-1}$ versus time for a typical experiment is shown in Fig. 6. The data are well described by a straight line, and the second-order rate coefficient obtained from the slope is equal within experimental uncertainty to the value of $2k_3$ obtained from the data with N_2 as the bath gas (see above). We conclude that our data show no evidence for a reaction between CS_2–Cl and O_2. In order to put a reasonable upper limit on k_2, kinetic simulations were carried out for a simple two-reaction scheme, i.e., reactions (2) and (3), with $2k_3$ fixed at the value obtained from the slope of $[CS_2–Cl]^{-1}$ versus time plot and k_2 varied. Plotted in Fig. 6 are simulated temporal profiles for $k_2 = 0.5$, 1.0, and 2.0×10^{-17} cm^3 molecule^{-1} s^{-1}. We conclude that upward curvature in $[CS_2–Cl]^{-1}$ versus time plot would have been observed if $k_2 > 5.0 \times 10^{-18}$ cm^3 molecule^{-1} s^{-1}, and we adopt this value as the upper limit for k_2 that is consistent with our data.

As discussed above, little or no ClCO is thought to be generated from 248 nm photolysis of Cl_2CO. In the presence of 200 Torr O_2 at 240 K, any thermalized ClCO that was produced would rapidly react with O_2 to generate ClC(O)OO [42]. The UV absorption spectrum of ClC(O)OO has recently been observed in cryogenic matrices [43]; this species absorbs only very weakly to the red of 300 nm and did not interfere with the detection of CS_2–Cl in this study even if it was generated with significant yield. In back-to-back experiments where we interchange N_2 and O_2 as the bath gas but experimental conditions otherwise remain constant, the observed peak transient absorbance remains unchanged within experimental uncertainty. This observation is consistent with other evidence that supports prompt production of Cl with a quantum yield of 2.0 from Cl_2CO photolysis.

Nicovich et al. [32] studied the effect of added O_2 on $Cl + CS_2 \leftrightarrow CS_2–Cl$ equilibration kinetics and concluded that $k_2 < 2 \times 10^{-15}$ cm^3 molecule^{-1} s^{-1} at $T = 230$ K and $P = 30$ Torr O_2. Wallington et al. [33] used their measured upper limit "effective" rate coefficient of 4×10^{-15} cm^3 molecule^{-1} s^{-1} for CS_2 reaction with Cl at 298 K in 700 Torr air in conjunction with values for k_1 and k_{-1} reported by Nicovich et al. [32] to deduce the upper limit rate coefficient k_2 (298 K) $< 8 \times 10^{-17}$ cm^3 molecule^{-1} s^{-1}. Hence, the observations reported in this paper reduce the upper limit value for k_2 by a factor of 16 compared to the limits reported previously, although it is worth noting that our data were obtained at 240 K, while the upper limit reported by Wallington et al. [33] is based on data at 298 K, but requires extrapolation of Nicovich et al. results to higher temperature and pressure in order to obtain estimates for k_1 and k_{-1} at $P = 700$ Torr air and $T = 298$ K.

3.5. Kinetics of CS_2–Cl reactions with NO and NO_2

The reactions of CS_2–Cl with NO and NO_2 were studied at $T = 240$ K and $P = 30$ Torr (N_2 bath gas) under pseudo-first-order conditions with $[NO_x] \gg [CS_2–Cl]$.

$$CS_2–Cl + NO \rightarrow \text{products} \quad (5)$$

$$CS_2–Cl + NO_2 \rightarrow \text{products} \quad (6)$$

The reagent concentrations (in units of molecules cm^{-3}) used in these experiments were as follows: $[Cl_2CO] = 1.5 \times 10^{15}$; $[Cl]_0 = (2–4) \times 10^{12}$; $[CS_2] \approx 3 \times 10^{17}$; $[NO] = (2–26) \times 10^{14}$; $[NO_2] = (1–25) \times 10^{14}$. Relatively low-radical concentrations were employed in order to minimize the effect of radical–radical side reactions, i.e., reactions (3) and (4), on the observed absorbance temporal profiles. Experimental conditions of high $[CS_2]$, low temperature, and low pressure minimized the contribution of Cl reactions with NO and NO_2 to observed CS_2–Cl kinetics.

$$Cl + NO + M \rightarrow ClNO + M \quad (7)$$

$$Cl + NO_2 + M \rightarrow ClNO_2 + M \quad (8a)$$

$$Cl + NO_2 + M \rightarrow ClONO + M \quad (8b)$$

For $[CS_2] \approx 3 \times 10^{17}$ molecules cm^{-3} and $T = 240$ K, the equilibrium concentration of CS_2–Cl exceeds that of Cl by more than a factor of 30 [32].

As typified by the data shown in Fig. 7, absorbance decays were exponential, i.e., plots of ln A versus time were linear, as would be expected under the experimental conditions employed (see above). Measured pseudo-first-order decay rates (k_d), obtained from the slopes of plots like the one shown in Fig. 7, are plotted as a function of $[CS_2]$ in Fig. 8. The slopes of k_d versus $[CS_2]$ plots give the following second-order rate coefficients in units of 10^{-11} cm^3 molecule^{-1} s^{-1}: $k_5 = 2.17 \pm 0.07$ and $k_6 = 1.33 \pm 0.09$; uncertainties are 2σ and represent precision only. The NO_2 concentration data plotted in Fig. 8 are corrected for dimer formation assuming

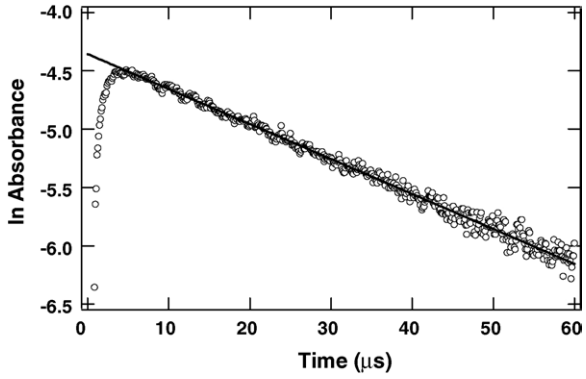

Fig. 7. Typical absorbance (base e) temporal profile observed following 248 nm laser flash photolysis of $Cl_2CO/CS_2/NO_x/N_2$ mixtures at $T = 240$ K and $P = 30$ Torr. The data shown were obtained with $NO_x = NO_2$. Concentrations in units of 10^{13} molecules cm^{-3} are $[CS_2] = 19000$, $[NO_2] = 259$, $[Cl_2CO] = 150$, and $[Cl]_0 \approx 0.36$. The solid line is obtained from a linear least squares analysis of the ln absorbance (A) vs. time (t) data at $t > 5$ μs; its slope gives the pseudo-first-order decay rate 29,900 s^{-1}.

a 240 K equilibrium constant of 6.2×10^{-17} cm^3 $molecule^{-1}$ for $NO_2 + NO_2 \leftrightarrow N_2O_4$ [44]; the magnitude of the correction ranged from 0.6% to 14% for the range of NO_2 concentrations employed to measure k_6. The value for k_6 reported above is derived under the (certainly valid) assumption that CS_2–Cl is much less reactive toward the closed shell species N_2O_4 than it is toward the open shell species NO_2.

For $[Cl]_0 \leq 4 \times 10^{12}$ per cm^3 (see above), reactions (3) and (4) contribute <600 s^{-1} to the early time part of observed decays and even less at longer times after the flash. Since most measured decay rates exceeded 10,000 s^{-1} (see Fig. 8), we conclude that the occurrence of radical–radical side reactions does not compromise the accuracy of the reported values for k_5 and k_6. At $T = 240$ K and $P = 30$ Torr N_2, $k_7 \sim 1.5 \times 10^{-13}$ cm^3 $molecule^{-1}$ s^{-1} [45] and $k_{8a} + k_{8b} \equiv k_8 \sim 2 \times 10^{-12}$ cm^3 $molecule^{-1}$ s^{-1} [46]. In our experiments, about 30% of the bath gas was CS_2, which is more efficient than N_2 as a third body. Hence, k_7 and k_8 are a little faster under our experimental conditions than the literature values given above. Nonetheless, it is clear that the values for k_5 and k_6 reported in this study are much faster than the known values for k_7 and k_8; this observation, along with the establishment of experimental conditions where the equilibrium concentration of CS_2–Cl was much greater than the equilibrium concentration of Cl, leads to the conclusion that reactions (7) and (8) made negligible contributions to CS_2–Cl kinetics in this study. To our knowledge, no kinetic data are reported in the literature for the reaction of Cl atoms with N_2O_4. However, given that (i) a relatively small fraction of NO_2 existed in the dimer form under the experimental conditions employed (see above); and (ii) Cl is almost certainly much more reactive with NO_2 than with N_2O_4, it seems safe to assume that the $Cl + N_2O_4$ reaction had a negligible influence on CS_2–Cl kinetics in this study.

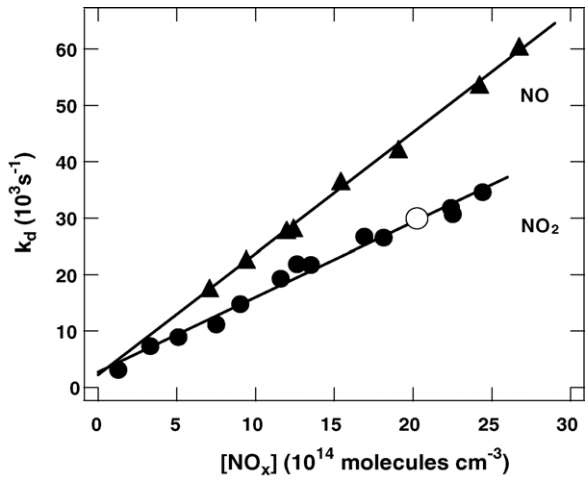

Fig. 8. Plots of pseudo-first-order adduct decay rate (k_d) vs. [NO_x] for data obtained at $T = 240$ K and $P = 30$ Torr N_2. Solid lines are obtained from linear least squares analyses; their slopes give rate coefficients (in units of 10^{-11} cm^3 $molecule^{-1}$ s^{-1}) of 2.17 ± 0.07 and 1.33 ± 0.09 for the reactions of CS_2–Cl with NO and NO_2, respectively (uncertainties are 2σ and represent precision only). The open circle is the data point that represents the data shown in Fig. 7.

Since side reactions have little or no impact on the accuracy of the reported rate coefficients, it appears that accuracy is limited by precision and by the accuracy with which the concentrations of NO and NO_2 are known (estimated to be ±5% for each). Hence, we report the rate coefficients $k_5 = (2.2 \pm 0.5) \times 10^{-11}$ cm^3 $molecule^{-1}$ s^{-1} and $k_6 = (1.3 \pm 0.4) \times 10^{-11}$ cm^3 $molecule^{-1}$ s^{-1}, where the uncertainties represent accuracy at the 95% confidence level.

Although there are no other reported measurements of k_5 and k_6 with which to compare our results, it is of interest to note that the rate coefficients reported in this study are very similar in magnitude to the rate coefficients for the reactions of $(CH_3)_2S$–Cl with NO and NO_2 (1.2×10^{-11} and 2.7×10^{-11} cm^3 $molecule^{-1}$ s^{-1}, respectively) that were measured by Urbanski and Wine using a technique analogous to the one employed in this study [34]. Urbanski and Wine also observed no reactivity of $(CH_3)_2S$–Cl with O_2. In a recent conference presentation, similar results have also been reported for reactions of $(CH_3)_2(O)S$–Cl with NO, NO_2, and O_2, i.e., in units of 10^{-11} cm^3 $molecule^{-1}$ s^{-1} rate coefficients are 1.5, 1.9, and $<1 \times 10^{-7}$, respectively [47]. It appears that Cl adducts to sulfur compounds react rapidly with compounds like NO and NO_2, where transfer of the chlorine atom to generate ClNO, $ClNO_2$, or ClONO is energetically favorable. Because Cl–OO is bound by only ~20 kJ mol^{-1} [48], the chlorine transfer reaction between the sulfur adducts and O_2 cannot occur at $T < 300$ K. While thermochemistry can explain why NO and NO_2 are highly reactive and O_2 is unreactive toward chlorine adducts with sulfur compounds, there appears to be little correlation between the rate coefficients and adduct bond strength for the energetically favorable NO_x reactions. All the adduct + NO_x rate coefficients summarized above are similar in magnitude even though the S–Cl bond strengths (at 0 K) are quite different (37 ± 6 kJ mol^{-1}

for SCS–Cl [25,32], $72 \pm 4\,kJ\,mol^{-1}$ for $(CH_3)_2(O)S–Cl$ [47,49], and $85 \pm 12\,kJ\,mol^{-1}$ for $(CH_3)_2S–Cl$ [8,50,51]). Diau and Lee have deduced rate coefficients for the reactions of $CS_2–OH$ with NO and NO_2 by examining the effect of added NO_x on $OH + CS_2 \leftrightarrow CS_2–OH$ equilibration kinetics [52]; they obtain a very fast rate coefficient ($4.2 \times 10^{-11}\,cm^3\,molecule^{-1}\,s^{-1}$) for the $CS_2–OH + NO_2$ reaction, but a much slower rate coefficient ($7.3 \times 10^{-13}\,cm^3\,molecule^{-1}\,s^{-1}$) for the $CS_2–OH + NO$ reaction. A mechanistic understanding of the differences in reactivity of NO and NO_2 toward $CS_2–OH$ remains to be developed.

3.6. Role of $CS_2–Cl$ in atmospheric chemistry

In the marine boundary layer (MBL), Cl concentrations are typically 10^4 atoms cm^{-3} [53] and have been reported to be as high as 10^5 atoms cm^{-3} in some locations [54]; these concentrations are 10–100 times lower than typical daytime OH levels, but are higher than Cl concentrations in other regions of the troposphere [55]. On the other hand, the rate coefficient for Cl addition to CS_2 is a factor of 5–10 faster than the rate coefficient for OH addition to CS_2 under typical MBL conditions ($P \sim 1$ atm; $250\,K < T < 310\,K$) [12,32]. Removal of CS_2 by OH is a relatively efficient process in the atmosphere because the $CS_2–OH + O_2$ reaction competes favorably with adduct thermal decomposition under atmospheric conditions [9–24]. The results reported in this paper suggest that under MBL conditions the lifetime of $CS_2–Cl$ toward reaction with O_2 is >0.025 seconds and the lifetime of $CS_2–Cl$ toward photo-dissociation is several seconds (even under the assumptions of unit photo-dissociation quantum yield and 0° zenith angle). Since the $CS_2–Cl$ lifetime toward thermal decomposition back to $CS_2 + Cl$ is $<10^{-5}$ s under MBL conditions [32], it is clear that the $Cl + CS_2$ association reaction will be of negligible importance as a destruction pathway for CS_2 in the atmosphere.

Acknowledgment

This research was supported by the National Science Foundation through grant ATM-03-50185.

References

[1] G.A. Russell, J. Am. Chem. Soc. 80 (1958) 4987–4996.
[2] G.A. Russell, J. Am. Chem. Soc. 80 (1958) 4997–5001.
[3] C. Walling, M.F. Mayahi, J. Am. Chem. Soc. 81 (1959) 1485–1489.
[4] J.E. Chateauneuf, J. Am. Chem. Soc. 115 (1993) 1915–1921.
[5] D. Wang, Y.-L. Li, W.S. Ho, K.H. Leung, D.L. Phillips, J. Org. Chem. 67 (2002) 747–752.
[6] P. Marshall, J. Mol. Struct. (Theochem) 236 (1991) 309–319.
[7] M.L. McKee, Chem. Phys. Lett. 209 (1993) 195–200.
[8] C. Wilson, D.M. Hirst, J. Chem. Soc., Faraday Trans. 93 (1997) 2831–2837.
[9] B.M.R. Jones, J.P. Burrows, R.A. Cox, S.A. Penkett, Chem. Phys. Lett. 88 (1982) 372–376.
[10] B.M.R. Jones, R.A. Cox, S.A. Penkett, J. Atmos. Chem. 1 (1983) 65–86.
[11] I. Barnes, K.H. Becker, E.H. Fink, A. Reimer, F. Zabel, H. Niki, Int. J. Chem. Kinet. 15 (1983) 631–645.
[12] A.J. Hynes, P.H. Wine, J.M. Nicovich, J. Phys. Chem. 92 (1988) 3846–3852.
[13] V.P. Bulatov, S.G. Cheskis, A.A. Iogansen, P.V. Kulakov, O.M. Sarkisov, E. Hassinen, Chem. Phys. Lett. 153 (1988) 258–262.
[14] E.R. Lovejoy, K.S. Kroeger, A.R. Ravishankara, Chem. Phys. Lett. 167 (1990) 183–187.
[15] T.P. Murrells, E.R. Lovejoy, A.R. Ravishankara, J. Phys. Chem. 94 (1990) 2381–2386.
[16] E.R. Lovejoy, T.P. Murrells, A.R. Ravishankara, C.J. Howard, J. Phys. Chem. 94, 2386–2393.
[17] S. Lunell, M.-B. Huang, K.A. Sahetchian, C. Chachaty, F. Zabel, J. Chem. Soc., Chem. Commun. (1990) 949–951.
[18] K.H. Becker, W. Nelsen, Y. Su, K. Wirtz, Chem. Phys. Lett. 168 (1990) 559–563.
[19] E.W.-G. Diau, Y.-P. Lee, J. Phys. Chem. 95 (1991) 379–386.
[20] M.L. McKee, Chem. Phys. Lett. 201 (1993) 41–46.
[21] R.E. Stickel, M. Chin, E.P. Daykin, A.J. Hynes, P.H. Wine, T.J. Wallington, J. Phys. Chem. 97 (1993) 13653–13661.
[22] E.R. Lovejoy, A.R. Ravishankara, C.J. Howard, Int. J. Chem. Kinet. 26 (1994) 551–560.
[23] L. Zhang, Q.-Z. Qin, J. Mol. Struct. (Theochem) 531 (2000) 375–379.
[24] M.L. McKee, P.H. Wine, J. Am. Chem. Soc. 123 (2001) 2344–2353.
[25] D. Wang, D.L. Phillips, Chem. Phys. Lett. 362 (2002) 205–209.
[26] M. Chin, D.D. Davis, Global Biogeochem. Cycles 7 (1993) 321–337.
[27] H. Berresheim, P.H. Wine, D.D. Davis, in: H.B. Singh (Ed.), Composition, Chemistry, and Climate of the Atmosphere, Van Nostrand Reinhold, New York, 1995, pp. 251–307.
[28] P.J. Crutzen, Geophys. Res. Lett. 3 (1976) 73–76.
[29] C.E. Junge, C.W. Chagnon, J.E. Manson, J. Meteorol. 18 (1961) 81–108.
[30] S.P. Urbanski, P.H. Wine, in: Z.B. Alfassi (Ed.), S-Centered Radicals, John Wiley & Sons, New York, 1999, pp. 97–140.
[31] D. Martin, I. Barnes, K.H. Becker, Chem. Phys. Lett. 140 (1987) 195–199.
[32] J.M. Nicovich, C.J. Shackelford, P.H. Wine, J. Phys. Chem. 94 (1990) 2896–2903.
[33] T.J. Wallington, J.M. Andino, A.R. Potts, P.H. Wine, Chem. Phys. Lett. 176 (1991) 103–108.
[34] S.P. Urbanski, P.H. Wine, J. Phys. Chem. A 103 (1999) 10935–10944.
[35] Z. Zhao, R.E. Stickel, P.H. Wine, Chem. Phys. Lett. 251 (1996) 59–66.
[36] H. Xu, J.A. Joens, Geophys. Res. Lett. 20 (1993) 1035–1037.
[37] E.G. Estupinan, J.M. Nicovich, P.H. Wine, J. Phys. Chem. A 105 (2001) 9697–9703.
[38] C. Maul, T. Haas, K.-H. Gericke, F.J. Comes, J. Chem. Phys. 102 (1995) 3238–3247.
[39] J.M. Nicovich, K.D. Kreutter, P.H. Wine, J. Chem. Phys. 92 (1990) 3539–3544.
[40] J.M. Nicovich, S. Wang, P.H. Wine, Int. J. Chem. Kinet. 27 (1995) 359–368.
[41] C.A. Piety, R. Soller, J.M. Nicovich, M.L. McKee, P.H. Wine, Chem. Phys. 231 (1998) 155–169.
[42] A.D. Hewitt, K.M. Brahan, G.D. Boone, S.A. Hewitt, Int. J. Chem. Kinet. 28 (1996) 763–771.
[43] H. Pernice, P. Garcia, H. Willner, J.S. Francisco, F.P. Mills, M. Allen, Y.L. Yung, Proc. Natl. Acad. Sci. U.S.A. 101 (2004) 14007–14010.
[44] S.P. Sander, R.R. Friedl, A.R. Ravishankara, D.M. Golden, C.E. Kolb, M.J. Kurylo, R.E. Huie, V.L. Orkin, M.J. Molina, G.K. Moortgat, B.J. Finlayson-Pitts, Chemical kinetics and photochemical data

for use in atmospheric studies, Evaluation 14, JPL Publication 02-25, 2003. http://jpldataeval.jpl.nasa.gov.
[45] J.H. Lee, J.V. Michael, W.A. Payne Jr., L.J. Stief, J. Chem. Phys. 68 (1978) 5410–5413.
[46] A.R. Ravishankara, G.J. Smith, D.D. Davis, Int. J. Chem. Kinet. 20 (1988) 811–814.
[47] P.H. Wine, J.M. Nicovich, M.L. McKee, K.M. Kleissas, S. Parthasarathy, F.T. Pope, A.T. Pegus, Proceedings of the 18th International Symposium on Gas Kinetics, Bristol, UK, Book of Abstracts, 2004, p. 21.
[48] See for example J.M. Nicovich, K.D. Kreutter, C.J. Shackelford, P.H. Wine, Chem. Phys. Lett. 179 (1990) 367–373.
[49] S. Vandresen, S.M. Resende, J. Phys. Chem. A 108 (2004) 2284–2289.
[50] K.C. Thompson, C.E. Canosa-Mas, R.P. Wayne, Phys. Chem. Chem. Phys. 4 (2002) 4133–4139.
[51] S. Enami, Y. Nakano, S. Hashimoto, M. Kawasaki, S. Aloisio, J.S. Francisco, J. Phys. Chem. A 108 (2004) 7785–7789.
[52] E.W.-G. Diau, Y.-P. Lee, J. Phys. Chem. 95 (1991) 7726–7732.
[53] O.W. Wingenter, M.K. Kubo, N.J. Blake, T.W. Smith Jr., D.R. Blake, F.S. Rowland, J. Geophys. Res. 101 (1996) 4331–4340.
[54] C.W. Spicer, E.G. Chapman, B.J. Finlayson-Pitts, R.A. Plastridge, J.M. Hubbe, J.D. Fast, C.M. Berkowitz, Nature (London) 394 (1998) 353–356.
[55] See for example O.W. Wingenter, D.R. Blake, N.J. Blake, B.C. Sive, F.S. Rowland, E. Atlas, F. Flocke, J. Geophys. Res. 104 (1999) 21819–21828.